

PACS numbers: 42.55.Ks; 42.60.Lh
DOI: 10.1070/QE2001v031n06ABEH001991

Study of the dynamics of spatial–energy and spectral characteristics of a cw chemical HF laser with a three-jet nozzle array

I A Fedorov, S V Konkin, Yu P Maksimov, A A Belyaev, N E Tret'yakov, A L Etsina

***Abstract*. The development of spatial – energy and spectral characteristics of a cw chemical HF laser with a three-jet nozzle array that was built using the nozzle – nozzle – nozzle mixing scheme is experimentally studied as a function of the degree of secondary dilution of the active medium with helium. The energy and spectral characteristics of laser emission were found to be unstable in time and dependent on the cavity configuration. The length of the lasing region upon the secondary dilution reached 10 – 12 cm, whereas the spacing between the onset of this region and the edge of the nozzle array was independent of the degree of dilution. The possibility of selecting spectral lines by varying the position of the optical cavity axis and the degree of secondary dilution was demonstrated.**

Keywords: *chemical laser, nozzle array, spatial – energy characteristics.*

1. Introduction

In Refs [1, 2], where a supersonic cw chemical HF laser with a three-jet nozzle array using the nozzle – nozzle – nozzle mixing scheme was numerically and experimentally studied, it was shown that the additional (secondary) dilution of the active medium (AM) with an inert gas (helium), which was supplied directly into the AM formation region, efficiently controlled such laser characteristics as the length of the lasing region, the spacing between the onset of this region and the edge of the nozzle array, the specific output energy, and the radiation power distribution over the beam cross section. In particular, the lasing region with a maximum length of 11 cm was detected by the method [3] using a double slit cavity, and an output laser beam with a nearly square cross section of size 10 cm × 11 cm was obtained in a laser with a wide-aperture stable plane – spherical cavity.

The study of the dynamics of spatial – energy characteristics of emission of such a laser in the near-field zone is of great interest for a detailed analysis of the operation of this laser. Such information can be obtained with the help of a scanning beam analyser, which was used in the study reported here. We used this instrument to study the time evolution of geometrical dimensions of the cross section of a laser beam, the power density distribution in this section, and the orientation of the lasing region relative to the edge of the nozzle array as functions of the degree of secondary dilution of the AM for different cavity configurations. The lasing spectra observed in different regions of the AM were simultaneously studied.

I A Fedorov, S V Konkin, Yu P Maksimov, A A Belyaev, N E Tret'yakov, A L Etsina 'Applied Chemistry' Russian Scientific Centre, prosp. Dobrolyubova 14, 197198 St. Petersburg, Russia

Received 29 January 2001
Kvantovaya Elektronika **31** (6) 515 – 519 (2001)
Translated by A N Kirkin

2. Experimental

We performed the experiments with an autonomous kilowatt supersonic cw HF laser with a 3-jet nozzle array that was built using the nozzle – nozzle – nozzle mixing scheme with a 16-mm nozzle step and an output cross section of size 11 cm × 40 cm [2]. The laser was placed in a low-pressure chamber, which was used for separating the free gas flow outgoing from the nozzle array from the environment. The working reagents represented gaseous deuterium, fluorine, helium, and hydrogen in the molecular proportion $D_2 : F_2 : He : H_2 : He^* = 1 : \alpha_1 : \psi_1(\alpha_1 - 1) : \alpha_2(\alpha_1 - 1) : \psi_2(\alpha_1 - 1)$ with the total mass flow $m = 105 - 125$ g s^{-1}. In the experiments, some dimensionless coefficients were fixed ($\psi_1 \sim 10$, $\alpha_2 \sim 40$), and the remaining coefficients were varied ($\alpha_1 = 1.54 - 1.77$, $\psi_2 = 0 - 9$).

We used three types of laser cavities (Fig. 1). The two-aperture cavity represented a double slit system [3], which was formed by independent cavities whose optical axes were parallel, but separated by the distance $\Delta x = x_2 - x_1 = 4.5$ cm along the direction of the AM flow. Each cavity had a rectangular aperture 11 cm high with the width $d_{1,2}$. A highly reflecting mirror represented a combination of two copper mirrors (*3*) and (*4*) with a radius of curvature of 5 m and contacting apertures of size $d_1 = 5$ cm and $d_2 = 4$ cm (Fig. 1a). An output mirror (*5*) represented a plane – parallel calcium fluoride plate 18 cm in diameter with a dielectric coating (30 % transmittance at 2.7 μm). The experiments were made for $x_1 = 2.5$, 4, and 6 cm. The laser output power (its longitudinal distribution) produced for these three cavity positions was used as a parameter characterising the AM length.

The plane – parallel Fabry – Perot cavity (Fig. 1b) was formed by a highly reflecting flat copper mirror (*9*) of size 15 cm × 30 cm, which was positioned outside the low-pressure chamber (*1*), and a plane – parallel plate (*5*). The stable plane – spherical cavity (Fig. 1c) consisted of a highly reflecting copper mirror (*10*) of size 15 cm × 15 cm with a radius of curvature of 20 m and a plane – parallel plate (*5*).

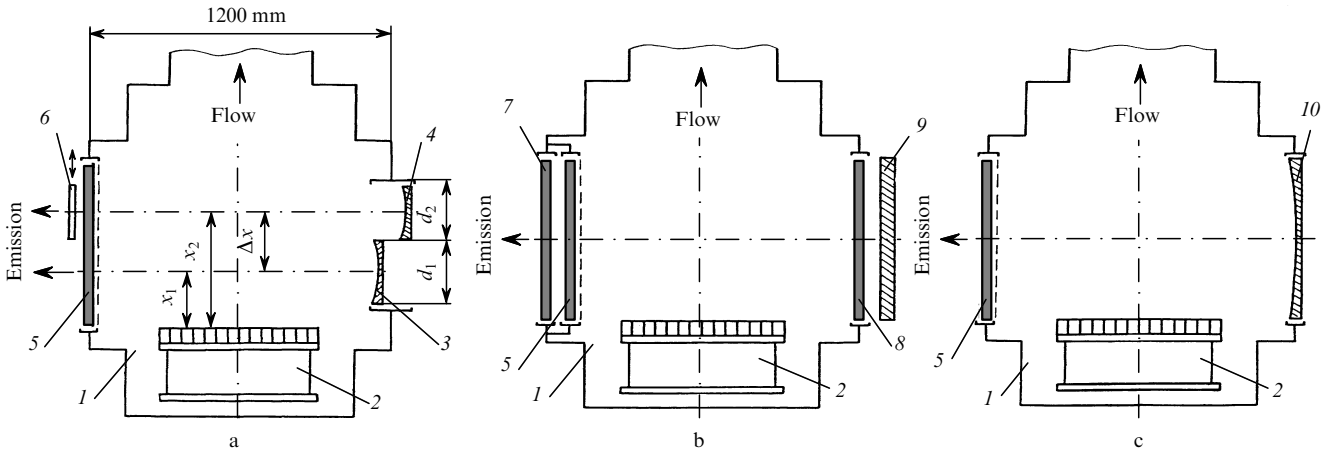

Figure 1. Schematics of the two-aperture slit (a), plane–parallel (b), and plane–spherical (c) optical cavities. (*1*) Low-pressure chamber; (*2*) cw HF chemical laser; (*3*, *4*, *10*) highly reflecting spherical mirrors; (*5*) outcoupling plane–parallel plate with a dielectric coating; (6) mechanical shutter; (*7*, *8*) protecting windows; (*9*) highly reflecting plane mirror.

In the experiments, we measured the output power N of the laser (with a fast PM-60 power converter with an error of ± 10 % and a fast UKPI-1 power converter with an error of ± 5 %) and the powers N_J of individual spectral lines (with a spectrometer on the basis of an IKM-1 monochromator). The spatial–energy characteristics of the laser output radiation formed in the plane–parallel and plane–spherical cavities were estimated in the near-field zone using a scanning beam analyser (the scanning was performed by using a pair of slits oriented in mutually perpendicular directions) [4]. The scanner readings were used for determining the radiation intensity distribution, the spacing between the onset of the lasing region and the edge of the nozzle array, and the length of this region.

3. Experimental results

The experiments were carried out in three stages. At each stage, we used a cavity of a certain configuration, which provided lasing with the secondary dilution of the AM with helium ($\psi_2 > 0$) and in the absence of the dilution ($\psi_2 = 0$).

3.1 Energy characteristics of laser radiation

For the laser operating with the two-aperture cavity, the output power outcoupled from each of the cavities was dependent on the oxidiser excess factor α_1. For $\alpha_1 < 1.7$, the output power outcoupled from the first (along the flow direction) cavity was higher than the output power from the second cavity. For $\alpha_1 > 1.7$, the output power was either comparable with the power outcoupled from the second cavity or lower. This dependence may be caused by the following. Our estimates show that excited HF(v) molecules cross the first cavity ($d_1 = 5$ cm) for $10^{-6} - 10^{-5}$ s, whereas their relaxation time under our experimental conditions is $\sim 10^{-7}$ s. Therefore, the excited molecules that have been formed in the first cavity and had no time to convert their energy into stimulated emission lose it through relaxation, enter the second cavity in the ground state, and are not involved in lasing. In the second cavity, laser radiation is produced exclusively by excited HF(v) molecules that are formed in it. Because the number of fluorine atoms acting as active centres in initiating the pumping reaction $F + H_2 \rightarrow HF(v) + H$ directly depends on the coefficient α_1, the higher is α_1, the larger is the number of fluorine atoms being produced and, therefore, the higher is the output power. As the secondary dilution coefficient ψ_2 is increased, the output radiation power increases from 5.7 kW (for $\psi_2 = 0$) to ~ 7 kW (for $\psi_2 = 8.5$). These results are somewhat worse than those obtained earlier in Ref. [2]. This may be caused by an unoptimised transmittance of the output mirror $\tau = 30$ % (in Ref. [2], it had a considerably lower transmittance $\tau = 18$ %).

The output power of the laser with the plane–spherical cavity was comparable to the value obtained for the two-aperture cavity, which supports the validity of our estimates. The output power of the laser with the plane–parallel cavity was low (below 2 kW), which is related to its configuration in which a protecting window (*8*), introducing considerable losses, was placed in front of the highly reflecting mirror (*9*) (Fig. 1b).

3.2 Spatial characteristics of the AM

It is known [1, 2] that the main consequences of the secondary dilution of the AM with helium (He^* molecules) are a decrease in the rates of diffusion of the jets of secondary fuel (H_2 molecules) into the flow of the oxidising gas (containing F atoms) of pump reactions and vibrational-energy relaxation, a decrease in the translational temperature of the AM, and, as a result, the retention of population inversion on a larger length. This fact is once again confirmed by the results of the experiments with the two-aperture cavity. As the coefficient ψ_2 is increased, the AM region with the maximum gain shifts downward the flow from the coordinate $x_{max} \sim 2.5$ cm (for $\psi_2 = 0$) to $x_{max} \sim 7$ cm (for $\psi_2 \sim 8.5$). Simultaneously, the far boundary of the AM shifts in the same direction almost by 1 cm from the coordinate $x_L = 10$ cm to $x_L = 11$ cm. These data agree well with the results obtained earlier in Ref. [2] and confirm their reliability.

The time dynamics of the spatial characteristics of the AM in the plane–parallel cavity is illustrated in Fig. 2. One can see that in both modes of laser operation, the onset of the lasing region, which is characterised by the coordinate x_0, is separated from the edge of the nozzle array (Figs 2a and 2b). For $\psi_2 = 0$, this separation is caused by a large distance between the axes of nozzles of the oxidising gas and the secondary fuel (a large nozzle step) and the presence of unfilled nozzles of secondary helium (the bottom effect). For $\psi_2 \sim 9$, the bottom regions are absent, but the reagent flows

are separated by an additional helium layer. Because the consequences of these effects are approximately identical, the spacing between the onset of the lasing region and the edge of the nozzle array in the two modes of laser operation is approximately the same, $x_0 = 1.1 - 1.2$ cm. The length Δx_L of the lasing region (Figs 2c and 2d) for $\psi_2 \sim 9$ is about 11 cm and exceeds the corresponding value for $\psi_2 = 0$ approximately by 2 cm. In the absence of secondary helium supply, the maximum of the longitudinal radiation intensity distribution corresponds to the coordinate $x_{max} = 8$ cm (Fig. 2e). In the presence of secondary dilution, this maximum shifts downward the flow to the coordinate $x_{max} = 18$ m (Fig. 2f). Because the distribution of radiation intensity on the output mirror of the plane–parallel cavity corresponds to the AM gain distribution, we used the dependences shown in Figs 2e and 2f to choose the optimum positions of the optical axis of the plane–spherical cavity for both modes of laser operation.

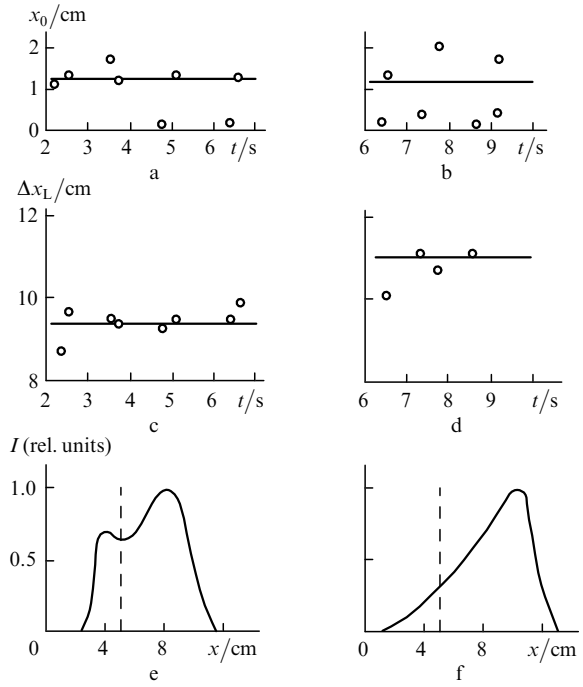

Figure 2. Time dynamics of spatial characteristics of the lasing region of the cw HF laser (a–d) and the radiation intensity distributions along the AM flow (e, f) for the laser with plane–parallel cavity and the secondary-dilution coefficients $\psi_2 = 0$ (a, c, e) and 9 (b, d, f).

The results illustrating the time dynamics of spatial characteristics of the lasing region in the plane–spherical cavity are shown in Fig. 3. The spacing between the onset of the lasing region and the edge of the nozzle array for two modes of laser operation is approximately the same (Figs 3a and 3b). The length Δx_L of the active region for $\psi_2 = 8.5$ (as in the case of the plane–parallel cavity) reaches 11 cm (Fig. 3d). For the plane–spherical cavity (Figs 3e and 3f), the nonuniformity of radiation intensity distribution on the output mirror along the active region is somewhat weaker than for the plane–parallel cavity. This difference is caused by the reversal (rotation) of the radiation field relative to its optical axis in the plane–spherical cavity, which somewhat improves the uniformity of the intensity distribution. Nevertheless, it follows from Figs 3e and 3f that in the presence of

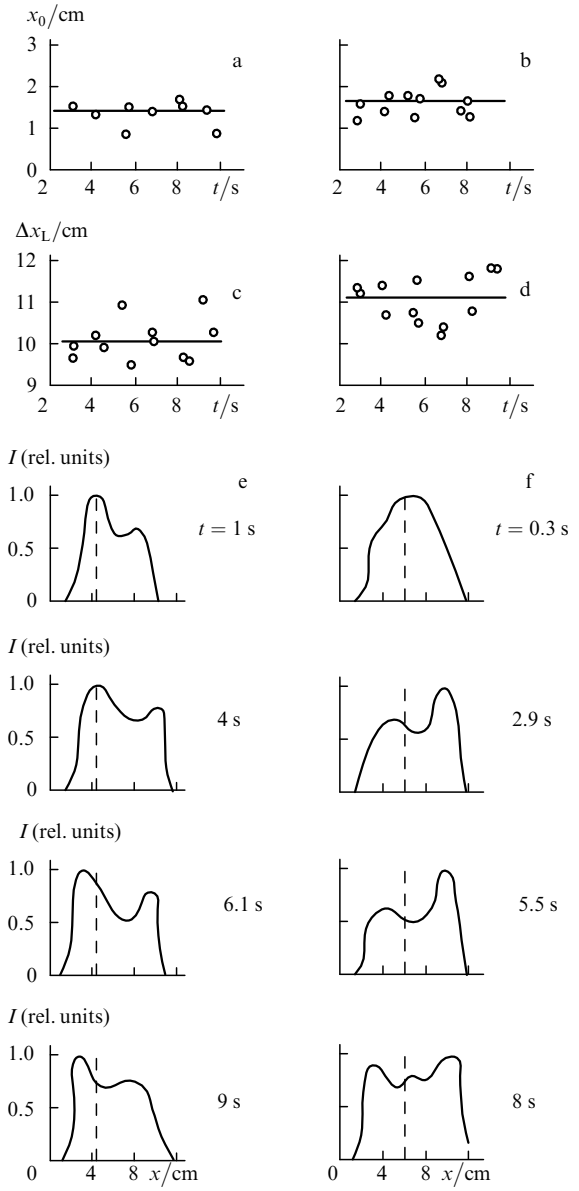

Figure 3. Time dynamics of spatial characteristics of the lasing region of the cw HF laser (a–d) and the radiation intensity distributions along the AM flow (e, f) for the laser with the plane–spherical cavity and the secondary-dilution coefficients $\psi_2 = 0$ (a, c, e) and 8.5 (b, d, f).

secondary dilution the maximum of the radiation intensity distribution shifts downward the flow, and the picture typical of the plane–parallel cavity (Figs 2e and 2f) is reproduced to a certain extent.

3.3 Spectral characteristics of laser emission

Fig. 4 presents the emission spectra (the relative powers of emission lines N_J/N, which are proportional to their intensities) for the 1–0 (thin lines) and 2–1 (thick lines) bands. In the initial region of the AM (Figs 4a–4c), when only the first slit cavity is used (Fig. 1, screen (*6*) shuts off the second cavity), the spectra demonstrate the redistribution of the radiation power among individual lines and their shift to the blue. Upon the secondary dilution (Figs 4b and 4c), the $P_0(5)$ and $P_1(4)$ lines appear and the maximum intensity is observed for the $P_0(6)$ and $P_1(5)$ lines (the subscripts of transition symbols correspond to the lower quantum state of an HF(v) molecule). This shows that the

translational temperature of the AM decreases. The relative intensity of spectral lines does not exceed 32 %.

The type of the spectra drastically changes (Figs 4d – 4i) with increasing distance from the observation point in the AM region to the edge of the nozzle array [for this purpose we used only the second cavity (Fig. 1); screen (*6*) shuts off the first cavity]. First, the spectral lines shift to the red. Second, the number of lines in each vibrational band decreases. Third, the emission energy is substantially redistributed among vibrational transitions in favour of the 2.774-μm $P_0(7)$ line, in which approximately 60 % of the energy is concentrated. The secondary dilution has only a weak effect on the shape of the spectra, by slightly decreasing (Figs 4d – 4f) or increasing (Figs 4g – 4i) the intensity of the $P_0(7)$ line.

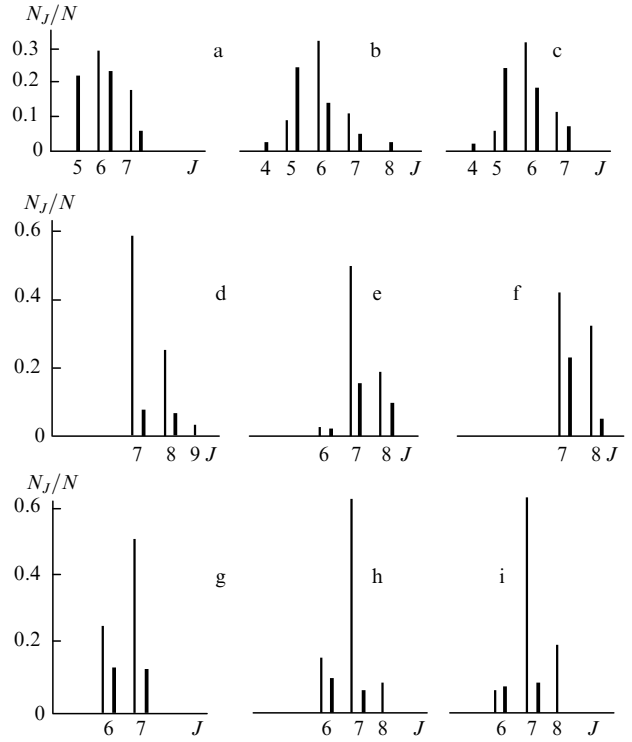

Figure 4. Emission spectra of the cw HF laser with the slit cavity measured at the distances $x = 2.5$ (a – c), 8.5 (d – f), and 10.5 cm (g – i) from the edge of the nozzle array for the secondary-dilution coefficients $\psi_2 = 0$ (a, d, g), 5 (b, e, h), and 8.5 (c, f, i).

This result is rather interesting. It points to the possibility of selection of spectral lines in a cw HF chemical laser with a three-jet nozzle array by varying the position of the optical cavity axis and the degree of secondary dilution of the AM with helium (the transmittance of the output mirror is fixed). In our study, the spectra of laser emission from the AM regions located at the distance greater than 8 cm from the edge of the nozzle array were recorded for the first time. One can see from Fig. 5 that in the absence of secondary dilution the longitudinal distribution of the parameter N_J/N for the $P_0(7)$ line has a maximum at a distance of 7 – 9 cm from the edge of the nozzle array (curve *1*). At larger distances, the $P_0(7)$ line intensity sharply decreases because of an increase in the translational temperature.

Upon the secondary dilution, the line intensity increases further with increasing distance from the nozzle array. The

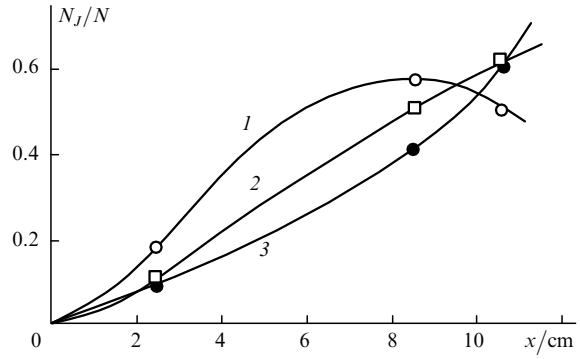

Figure 5. Longitudinal distributions of the parameter N_J/N for the $P_0(7)$ line for $\psi_2 = 0$ (*1*), 5 (*2*), and 8.5 (*3*).

higher the coefficient ψ_2, the higher the rate of the intensity increase (curves *2* and *3*). It is likely that in this case the negative effect of an increase in the translational temperature is compensated by the secondary dilution of the AM with helium. Note one more fact. The spectra presented in Fig. 4 were obtained for different coefficients α_1 ($\alpha_1 \sim 1.7$ in Fig. 4f and $\alpha_1 < 1.6$ in Fig. 4i). Because of this, the power of emission outcoupled from the second slit cavity differs from the power of emission outcoupled from the first cavity. Nevertheless, the total energy in the $P_0(7)$ and $P_0(8)$ lines reaches 80 % of the total emission energy.

As for the time stability of the spectra, the set of spectral lines and the ratio of their intensities are almost unchanged during at least first seven seconds of laser operation. Then, the number of lines is decreased and the emission energy is redistributed to the red. This effect may be caused by an increase in pressure in the low-pressure chamber and, therefore, in the AM (in the given case, from 2.5 to 4 Torr). Because the relation between the laser emission spectrum and the gas-dynamic parameters of the AM and the position of the optical cavity axis is studied insufficiently, these questions call for a further study.

The emission spectra of the cw HF chemical laser with the plane – spherical cavity (Fig. 6) were measured for two secondary dilution coefficients $\psi_2 = 0$ and 8.5, the optical cavity axis being located in both cases at the optimum distance from the edge of the nozzle array: $x_{opt} = 4.5$ cm for $\psi_2 = 0$ and $x_{opt} = 6$ cm for $\psi_2 = 8.5$. In the absence of secon-dary dilution (Figs 6a – 6c), the spectrum is more stable in time, both with respect to the set of lasing lines and their intensity. In the case of secondary dilution (Figs 6d – 6f), the spectrum is less stable and (as in the case of the slit cavity) the number of lines decreases and the emission power is redistributed to the red (in the present case, into to the $P_0(7)$ line) after 7 – 8 s of laser operation. This effect is explained above. Note that the intensities of the $P_0(7)$ line in Figs 6a and 6d exactly agree with the distributions obtained by scanning the active region with the slit cavity (Fig. 5, curves *1* and *3*).

4. Conclusions

The study of the dynamics of spatial – energy and spectral characteristics of the output emission of the cw HF chemical laser with the three-jet nozzle array using the nozzle – nozzle – nozzle scheme gave the following results:

(1) by using a two-aperture slit cavity, we obtained the radiation intensity distribution that confirms the earlier

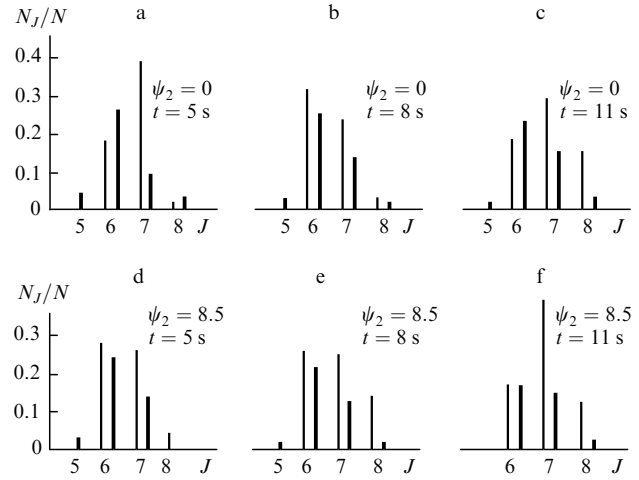

Figure 6. Emission spectra of the cw HF laser with the plane-spherical cavity measured for different secondary-dilution coefficients ψ_2 at different moments of time t.

results; we showed the possibility of selecting spectral lines by varying the position of the optical cavity axis and the degree of secondary dilution of the AM with helium, which made it possible to concentrate more than 60 % of emission power in the 2.744-μm $P_0(7)$ line;

(2) by using plane–parallel and plane–spherical cavities, we found that the spacing between the onset of the lasing region and the edge of the nozzle array is independent of the degree of secondary dilution of the AM with helium; the length of the lasing region reaches 10–12 cm; the distribution of energy characteristics of laser emission is unstable in time and depends on the cavity configuration (in the plane–parallel cavity, the distribution patterns are asymmetric about the alignment axis, and the shape of the intensity distribution in the plane–spherical cavity reflects the reversal of the radiation field relative to its axis, which represents the symmetry axis).

Acknowledgements. The authors thank V K Rebone for his help in the experiments and P G Lyashed'ko and V E Doroshkevich for their assistance in the measurements.

References

1. Rotinyan M A, Strelets M Kh, Fedorov I A, Shur M L *Kvantovaya Elektron.* **25** 387 (1998) [*Quantum Electron.* **28** 375 (1998)]
2. Konkin S V, Rebone V K, Fedorov I A, et al. *Kvantovaya Elektron.* **25** 397 (1998) [*Quantum Electron.* **28** 384 (1998)]
3. Galaev I I, Konkin S V, Fedorov I A, et al. *Prib. Tekh. Eksp.* (1) 122 (1997)
4. Malacara D (Ed.) *Optical Shop Testing* (New York: Wiley, 1978; Moscow: Mashinostroenie, 1985)